

An continuous attractors network model for grid-cell modules based on toroidal manifolds

Zhihui Zhang^{a,b,c}, Fengzhen Tang^{b,c,*}, Yiping Li^{b,c}, Xisheng Feng^{b,c}

^a*University of Science and technology of China, No.96, JinZhai Road Baohe District, Hefei, 230026, Anhui, China*

^b*The State Key Laboratory of Robotics, Shenyang Institute of Automation, Chinese Academy of Science, No.135, Chuangxin Road Hunnan District, Shenyang, 110016, Liaoning, China*

^c*Institutes for Robotics and Intelligent Manufacturing, Chinese Academy of Sciences, No.135, Chuangxin Road Hunnan District, Shenyang, 110169, Liaoning, China*

Abstract

Although grid cells in the entorhinal cortex are regarded to be a key component of spatial cognition in animals, the latent mechanisms of grid-cell firing are still up for discussion. Current main computational models of grid cells focus more on the activity of single grid cell. However, The evidence has suggested that the grid-cell activity was generally organized into a small number of discrete functional modules([Stensola et al., 2012](#)). Here, we proposed a continuous attractors network(CAN) model for grid-cell modules. The propose model not only can be driven using the self-motion input from the speed cells and head direction cells of animals but also it is injected energy by receiving the external cues via place cells. Consistent with the experiment results, every grid-cell neuron in the CAN can reproduce the hexagonal firing patterns with driving the model. Our model simultaneously shows the path integration capability that a grid-cell module is thought to have. Even when the animal lacks the correction of external cues, our model still predicts the prominent performance of path integration for grid-cell modules over long distances. In addition, our model also support the hypothesis([Gardner et al., 2022](#)) that the grid cells from an single module exist on a toroidal manifold.

Keywords: Grid cell, Place cell, Continuous attractors network, Path integration

1. Introduction

The spatial cognition is crucial for rodent animals to find food and return their nests. The concept of cognitive map first is proposed as an abstract map to represent the environment in the brain of animals([Tolman, 1948](#)). The entorhinal-hippocampal circuit is widely thought to provide the material foundation for cognitive([McNaughton et al., 2006](#)). Especially, the spatial relative cells including head direction cells, place cells, speed cells and grid cells are gradually discovered consecutively in the entorhinal-hippocampal circuit. The one of important discovery is grid cells in the medial entorhinal cortex(mEC)([Moser et al., 2017](#)) due to their special firing patterns. The grid cells have hexagonally arranged firing fields that can cover entire environment that a freely moving animal has passed through([Rowland et al., 2016](#)). In addition, the grid cells widely exist in many kinds of animals, including rat, mice([Fyhn et al., 2008](#)), bats([Yartsev et al., 2011](#)), monkey([Killian et al., 2012](#)) and human([Jacobs et al., 2013; Kunz et al., 2015; Doeller et al., 2010](#)). This shows that the grid cells widely exist in mEC as an important role in the cognitive map of rodent animals. Since the discovery of the grid cells, the function of them in cognitive map keep drawing attention to researchers all the time. One crucial problem of grid cells is the reason how the hexagonal firing patterns are formed. To explain it, many computational models are proposed. Current main computational

models contain oscillatory-interference (OI) models, Continuous attractor network (CAN) models and single-cell plasticity models.

Oscillatory-interference(OI) models of grid cells are proposed in the early 1990s to explain the origin of place field and their relationship with the hippocampal theta rhythm([O'Keefe and Burgess, 2005; Burgess et al., 2007; Hasselmo et al., 2007; Pastoll et al., 2013; Burgess, 2008](#)). The dual-oscillator model can explain the emergence of place fields and phase procession([O'Keefe and Burgess, 2005](#)). At the same time, it also can intrinsically generate periodic patterns. So it was used to try to explain the periodic firing fields of grid cells([D'Albis, 2018](#)). In this models, the periodic patterns are generated by interfering with multiple oscillators that have different frequencies. These oscillators with different frequencies are modulated by the moving speed and direction of the animals. So such oscillators are called velocity-controlled oscillators(VCO). By this, only two VCOs are enough to generate grid-like patterns. Although the OI models have been supported by some researches([Schmidt-Hieber and Häusser, 2013; Domnisoru et al., 2013; Welday et al., 2011; Koenig et al., 2011; Brandon et al., 2011; Giocomo et al., 2007; Hafting et al., 2005; Alonso and Llinás, 1989](#)), there are still some problem for OI theory. An problem of OI models is the 60 degree angle between multiple VCOs needs to be specified manually. Additionally, The grid-like patterns of OI models can be rapidly disrupted by noise([D'Albis, 2018](#)). Some experimental evidence also against OI models. Giocomo et al demonstrates that the intrinsic resonance is not required for grid patterns to form([Giocomo et al., 2011](#)). The grid-

*Corresponding author

like activity is observed without theta modulation in crawling bats.(Yartsev et al., 2011). And the membrane-potential dynamics of grid cells is inconsistent with a purely interference-based mechanism(Domnisoru et al., 2013). These evidence shows that the OI models may not be latent mechanism of grid-cell activity(Moser et al., 2017).

The single-cell plasticity models more emphasize the role of external sensory cues and learning process compared with other grid-cell models(D'Albis, 2018). The simplest single-cell plasticity model is proposed by Kropff and Treves(Kropff and Treves, 2008). They think the grid-cell firing patterns are formed by synaptic excitation and neural intrinsic competition. The competition could arise from the spike-rate adaptation. Then the Hebbian rules are utilized to imprint the synaptic connection in the output activity of the cell. The preferred spacing of grid cells are controlled by the time constant of spike-rate adaptation and the average running speed of the animal. The single-cell plasticity models leverage the inherent single-cell mechanism to explain the hexagonal firing patterns. However, the Kropff- Treves model CANot explain the common alignment within grid-cell modules(Hafting et al., 2005; Fyhn et al., 2008; Stensola et al., 2012). The later models try to add the recurrent collaterals and head-direction tuning(Kropff and Treves, 2008; Si et al., 2012) to give the desired network properties. In summary, the head-direction tuning is required for grid alignment during the development of grid patterns(Rowland et al., 2016).

The CAN models are another type of very influential models in the field of computational neuroscience. The fundamental premise of such models is that a correctly designed recurrent network may sustain a continuous stable states in its neurons activity(Taylor, 1999; Amari, 1977). Multiple CAN models of grid cells have been proposed to explain the grid-like patterns(Fuhs and Touretzky, 2006; Burak and Fiete, 2009; Guanella et al., 2007; Shipston-Sharman et al., 2016; Couey et al., 2013). They can roughly divided into two types including single-bump CANs and multiple-bump CANs. In the single-bump CANs, the networks only exist a bump at the same time(Guanella et al., 2007). The neurons in the networks are arranged using the preferred spacing and orientation of the grid cell. However, in multiple-bump CANs, there are multiple bumps of activity in the CAN of grid cells by the weight profile of Mexican-hat or Lincoln-hat(Rowland et al., 2016). Then the bumps in networks can be driven by self-motion cues. Rodents can utilize self-motion cues to navigate across short distances, which is consistent with the features of the CAN. And CAN have been witnessed to be in line with the modular organization of grid cell activity(Stensola et al., 2012; Yoon et al., 2013). The CAN models have been widely applied to multiple recognized cells in the entorhinal–hippocampal neuronal circuits, such as head direction cells and place cells. In addition, the CAN models is naturally suitable to process the path integration in cognitive map. So in the research area of cognitive map and robot navigation, the CAN models acquire more attention. However, to generate the hexagonal firing patterns, current CAN models of grid cells have obvious artifacts. For example, In (Guanella et al., 2007), the neurons in CAN are manually organized in a

plane covering the repetitive rectangular structure to generate the hexagonal firing patterns. Additionally, in (Guanella et al., 2007), the CAN models of grid cells receive the input from the CAN models of place cells connecting by the Hebbian rules.

As mentioned above, many computational models of grid cells are proposed to explain the grid patterns of individual grid cell. However, evidence have shown that grid-cell activity was discovered to be structured into a small number of distinct functional modules(Stensola et al., 2012). A recent research shows that grid-cell activity from a single module is distributed on a toroidal manifold, as expected in a two-dimensional CAN(Gardner et al., 2022). The current CAN models(Fuhs and Touretzky, 2006; Burak and Fiete, 2009; Guanella et al., 2007) of individual grid cells in the research are used to predict the activity of grid cells. It is consistent with the experimental data of grid cells to some extent. But current CAN models are designed for single grid cell. So there are some inconsistent between prediction of models and experimental data. The research demonstrates that the individual cells are preferentially active at singular position on the torus and the position on the torus correspond to position of the moving animal in the physical space(Gardner et al., 2022). However, for multiple-bump CAN models, the neurons are activated at the same time in several position on the torus. For single-bump CAN models, the neurons are ordered hexagonally and can not map animal's positions in the environment. So here, we focus on individual grid-cell module and propose a new CAN models for the grid-cell module. Because in a single module, all grid cells have same spacing and orientation(Stensola et al., 2012). So in our model of grid cells, the neurons that represented grid cells are arranged in a plane according to their own phases and formed 2D toroidal manifolds. So our CAN model is marked as Phase-CAN. In this way, the structure of the PhaseCAN is established like the CAN models of place cells(McNaughton et al., 2006). This improves the overall network structure's naturalness comparing with the CAN of grid-cell model(Guanella et al., 2007). In addition, we build a direct connection between place cell and grid-cell module using the spatial transformation. By this connection, the deviation of path integration can be corrected in the CAN model of grid cells based on phases. Then the activity of single grid cell in the CAN is recorded and shows the hexagonal firing patterns. It is consistent with the biological experiment about single grid-cell activity(Hafting et al., 2005). Finally, the performance of the path integration using our model is evaluated in different spacing, sizes of network, moving steps. The results demonstrate that our model performs very well across extended distances and without external cues. In addition, our model also supports the hypothesis about the activity of single grid-cell module(Gardner et al., 2022).

2. Results

2.1. The structure of proposed model

In the reference (Stensola et al., 2012), it shows that grid cells form discrete modules. And each grid module shares a common spacing, orientation(Rowland et al., 2016). Previous models of

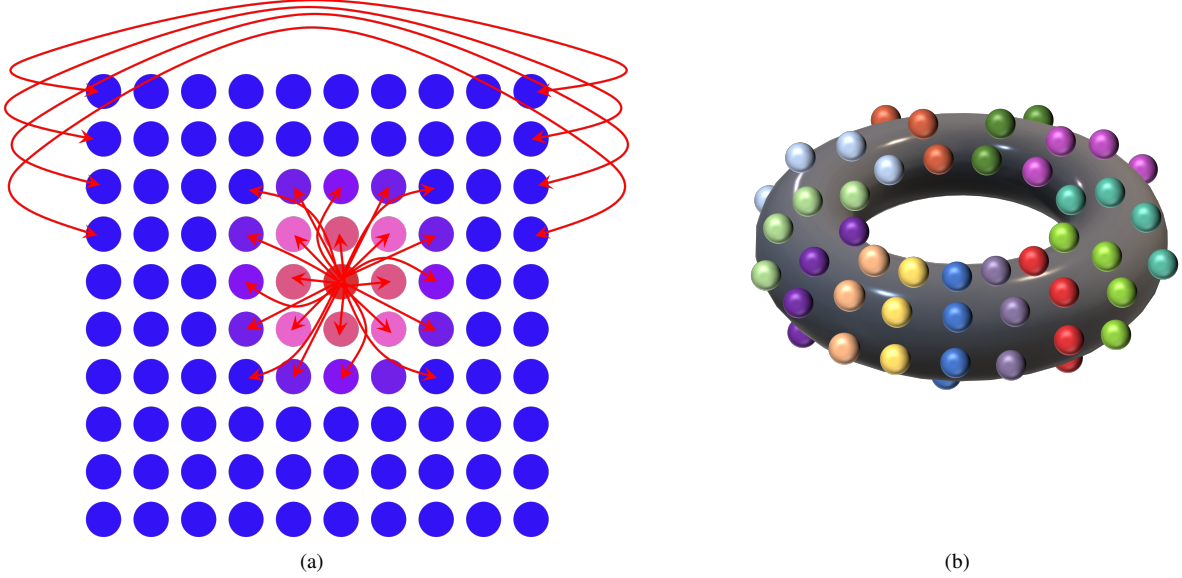


Figure 1: The structure of PhaseCAN. (a) The neurons in a singular grid-cell module are arranged on a sheet according to their phases. They are mutually connected by weight profile according to distance between them on the sheet. The distance between neurons needs to consider the periodic boundary condition. (b) The networks with periodic boundary condition can form toroidal manifold. In the toroidal manifold, the neurons are mutually connected according to their weights.

grid cells more focus on explaining the firing patterns of a single grid cell. Here, we concentrate on single grid-cell module and explore its firing mechanism. As Fig. 1(a) depicted, in our model, the neurons of grid cells in same module are arranged in a sheet. In this sheet, the population neurons are defined as follows:

$$M = N_x \times N_y \quad (1)$$

where N is the amount of the neurons of grid cells, N_x is the amount of the neurons in the horizontal direction, N_y is the amount of the neurons in the vertical direction. In our model, the relationship of N_x and N_y are defined by:

$$N_x = N_y = N \quad (2)$$

To simply demonstrate the proposed model, a grid cell can be represented as follows:

$$\mathbf{G}_i = [s_i, o_i, \boldsymbol{\vartheta}_i], i \in \mathbb{Z}^+ \quad (3)$$

where s_i represents the spacing of the grid cell \mathbf{G}_i , o_i represents the orientation of the grid cell \mathbf{G}_i , $\boldsymbol{\vartheta}_i$ represents the phase of the grid cell \mathbf{G}_i and $\boldsymbol{\vartheta}_i = [\vartheta_i^1, \vartheta_i^2]$ contains the phases of the two directions.

For the grid cells in a module, they share common spacing and orientation. So the grid cells of the same module can be further represented as follows:

$$\mathbf{G}_i = [s, o, \boldsymbol{\vartheta}_i], i \in \mathbb{Z}^+ \quad (4)$$

A grid cell \mathbf{G}_i in a module can be placed in the sheet according to its phases. Different from the CAN model in the reference(Guanella et al., 2007), all neurons ϵ_{xy} in our model

are arranged as a matrix instead of repetitive rectangular structure. According to the phases of the grid cell \mathbf{G}_i , the index (x, y) of a neuron ϵ_{xy} in the matrix can be described as follows:

$$\left\{ \begin{array}{l} x = \frac{\vartheta_i^1}{\Delta\vartheta^1} \\ y = \frac{\vartheta_i^2}{\Delta\vartheta^2} \end{array} \right. \quad (5)$$

$$\left\{ \begin{array}{l} x = \frac{\vartheta_i^1}{\Delta\vartheta^1} \\ y = \frac{\vartheta_i^2}{\Delta\vartheta^2} \end{array} \right. \quad (6)$$

where $\Delta\vartheta$ is the phase gap of neighbor neurons, ϑ_i^1 and ϑ_i^2 are the phases of \mathbf{G}_i . As Fig. 1(a) depicted, the neurons in our model are connected recurrently and have the periodic boundary condition. So the max phase of the neurons in the model is equal to the spacing of the grid module. Then $\Delta\vartheta$ can be further calculated as follows:

$$\Delta\vartheta = \frac{s}{N} \quad (7)$$

where s is the spacing of the grid-cell module, N is the size of the CAN model.

2.2. The connection of proposed model

As mentioned above, the grid cells neurons in identical module are arranged in a sheet. They are connected with each other and have periodic boundary condition. This is depicted in Fig. 1. For these grid cells that have same spacing and orientation in identical module according to (Burak and Fiete, 2009), the dynamic of rate-based neurons can be described by:

$$\tau \frac{dr_i}{dt} + r_i = f \left[\sum_j w_{ij} r_j \right] \quad (8)$$

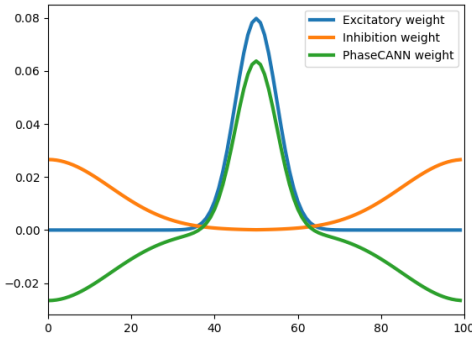


Figure 2: The weight profile of the PhaseCAN. The weight profile of the PhaseCAN consists of two part. One part is the excitatory weight to activate the local neurons. The another part is the inhibition part and it inhibit distant neurons. The two part is used to compute the weight profile of the PhaseCAN by Eq. (11).

where τ is the time-constant of neuron response, r_i is spike rate of the neuron, f is a non-linearity function and can be described as follows:

$$f(x) = \begin{cases} = x, x > 0 \\ = 0, \text{otherwise} \end{cases} \quad (9)$$

The w_{ij} in Eq. (8) is the connection weight from neurons ϵ_j and neuron ϵ_i . It includes two parts. The first part is used to exciting the neighbor neurons of the neuron ϵ_j . The second part is utilized to inhibit the neighbor neurons of the neuron ϵ_j . In here, two Gaussian function are used to generate the weight profile. The weight is depicted in Fig. 2. So w_{ij} can be described as follows:

$$w_{ij} = \alpha e^{-\rho d_{ij}^2} - \beta e^{-\gamma(d_{ij}-D)^2} \quad (11)$$

where w_{ij} is the weight from ϵ_j to ϵ_i , $\alpha, \rho, \beta, \gamma$ are the hyperparameters to adjust the scope of Gaussian function, D is the max distance of two neurons in the network, d is the distance between ϵ_j and ϵ_i and it can be computed as follows:

$$d_{ij} = \|\epsilon_i - \epsilon_j\|_2 \quad (12)$$

$$= \sqrt{(x_i - x_j)^2 + (y_i - y_j)^2} \quad (13)$$

2.3. Activity and stabilization

Place cells have been considered to provided the input for grid cells. The experiment that recorded the neural activity in the medial entorhinal cortex(MEC) of rat after temporary inactivation of the hippocampus shows that grid cells will lost their grid-like firing patterns and tune to the direction of the rat's head(?). To make gird cells acquire the input from the place cells, the CAN of place cells(McNaughton et al., 2006) is used to inject the activity to the PhaseCAN. As depicted in Fig. 3, for a landmark in the true world, it can be mapping to a neuron activity in the place cell sheet. According to our previous work, a landmark P_i^w was firstly transformed into place cell firing space by:

$$\mathbf{P}_i^p = \mathbf{R}_{wp} \cdot \mathbf{P}_i^w + \boldsymbol{\varpi}_i \quad (14)$$

where \mathbf{R}_{wp} and $\boldsymbol{\varpi}$ are the rotation matrix and translation vector. And \mathbf{R}_{wp} can be described by the rotation angle ϕ as follows:

$$\mathbf{R}_{wp} = \begin{bmatrix} \cos\phi & -\sin\phi \\ \sin\phi & \cos\phi \end{bmatrix}^{-1} \quad (15)$$

This can inject energy for place cell CAN model. Then the excitation can be updated according to the weights between place cells neurons in the sheet(?). After the process of competitive attractor network dynamics, the network of place cells gradually is stabilized. Then the neuron that have maximum firing rate is found and marked as \mathbf{P}_{\max}^p . It will be transform into grid cells firing space by:

$$\mathbf{P}_i^g = \mathbf{R}_{pg} \cdot \mathbf{P}_{\max}^p \quad (16)$$

where \mathbf{P}_i^g is the corresponding neuron position in the PhaseCAN, \mathbf{R}_{pg} is the transformation matrix and it can be depicted as follows:

$$\mathbf{R}_{pg} = \begin{bmatrix} s \cdot \cos(o_i) & s \cdot \cos(o_i + \pi/3) \\ s \cdot \sin(o_i) & s \cdot \sin(o_i + \pi/3) \end{bmatrix}^{-1} \quad (17)$$

where s and o separately is the spacing and orientation of the grid cell module. For the firing rate of \mathbf{P}_i^g , it can be calculated as follows:

$$\varsigma_i = \sum_{k=1}^M \mathcal{T}_{ik} \mathcal{F}(\mathbf{P}_k^p) \quad (18)$$

where ς_i is the firing rate of \mathbf{P}_i^g , M is the neural population of the place cell network, \mathcal{T}_{ik} is the weight profile that is learned by Hebbian rule, $\mathcal{F}(\cdot)$ is the function to acquire the firing rate of \mathbf{P}_k^p in the place cell network.

In this way, the PhaseCAN can acquire excitation from the external cues. So the firing rate of single neuron in the Eq. (8) can be further described as follows:

$$\tau \frac{dr_i}{dt} + r_i = f \left[\sum_j w_{ij} r_j + Q_i \right] \quad (19)$$

where Q_i is the feedforward input to neuron i from external cues. After receiving the external excitation, the PhaseCAN need to process the excitatory update. A two-dimension discrete Gaussian distribution is used to generate the excitatory weight matrix, w_{ij} , which is depicted in Eq. (11). Then each neuron uses it to project activity to all other neuron in the PhaseCAN.

Finally, the PhaseCAN is normalized to constrain the sum of activation in whole network. Before normalization, the firing rate of each neuron need to be maintained a scope by Heaviside function. Then the normalization process can be described as follows:

$$\tilde{\varsigma}_i = \frac{\varsigma_i}{\sum_{j=1}^N \varsigma_j} \quad (20)$$

where $\tilde{\varsigma}_i$ is the firing rate after normalization, N is the neuron population of PhaseCAN.

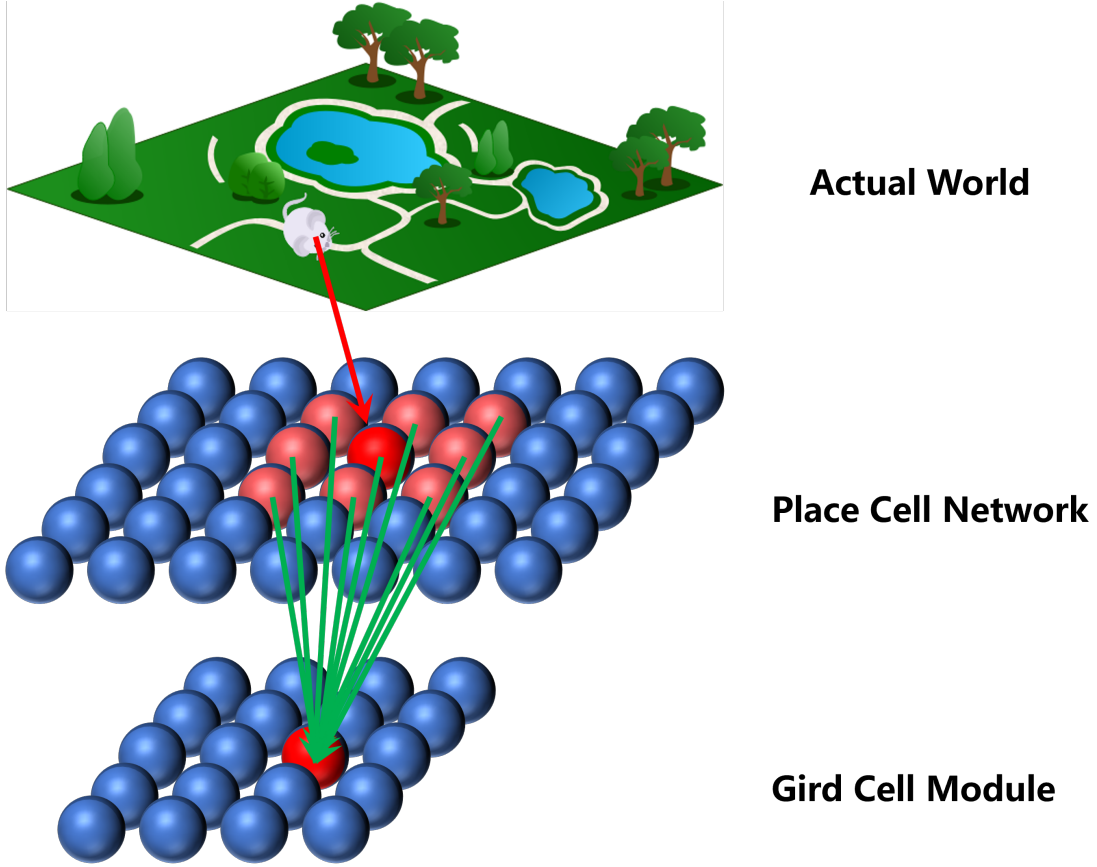


Figure 3: The grid cell module receives excitation from external cues. In the top of the figure, the rat moves in the actual world. The place cell CAN network and grid cell module are driven by the velocity and the head direction from the speed cells and head direction cell of the rat. When the rat receives the excitation from landmark, the bump position of the place cell network will be used to activate the grid cell module by the Eq. (18) and Eq. (16).

Table 1: The parameters of the PhaseCAN

Parameters	N_x	N_y	s	σ	α	β	ρ	$gamma$
value	100	100	1.0	$\pi/3$	1.0	1.0	0.01	0.003

To verify the ability of receiving the excitation of the network, a PhaseCAN was established according to 2.1 and 2.2. The parameters of the network mentioned are listed in Tab.1.

As the Fig. 4 depicted, multiple position was injected energy and the activity bump was formed by diffusing the excitation using the connection between neurons. In addition, latter position injected energy inhibited the former. For this reason, the former positions remain a dim bump in Fig. 4(b)-4(d). In addition, comparing the Fig. 4(b) and Fig. 4(c), the previous bump in center position will be disappeared with injecting energy in new position. This demonstrates that our model have suitable weight connection between neurons to perform excitation and inhibition. When the bump position is in the edge of network sheet, the bump will appear in the opposite edge of the sheet depicted in Fig. 4(c) and Fig. 4(d). This demonstrate the our model exist the periodic boundary condition.

2.4. Path integration

For the CAN models, the path integration is a important ability comparing with other models of grid cells. The path in-

tegration process updates the network activity by shifting the activated bump based on the velocities and head direction angles from speed cell(Kropff et al., 2015) and head direction cell(Zhang, 1996; ?). In general, the path integration in CAN models is performed by projecting existing neural bump to the future location and dynamically shifting the current activity to towards the future location. Another method of the path integration shifting existing neural bump rather than projecting a copy of the current activity. This approach makes the performance of the robot independent of varying sensory update rates and robot velocity, resulting in more precise robot trajectories and eliminating the need for parameter adjustment(?). Here, the latter method was chosen to process the path integration. However, different with (?), in here, the translation in the world frame needs to be transformed into PhaseCAN and the computation of firing rate is performed using the convolution kernel.

After the rat move a distance per unit time, the offsets can be

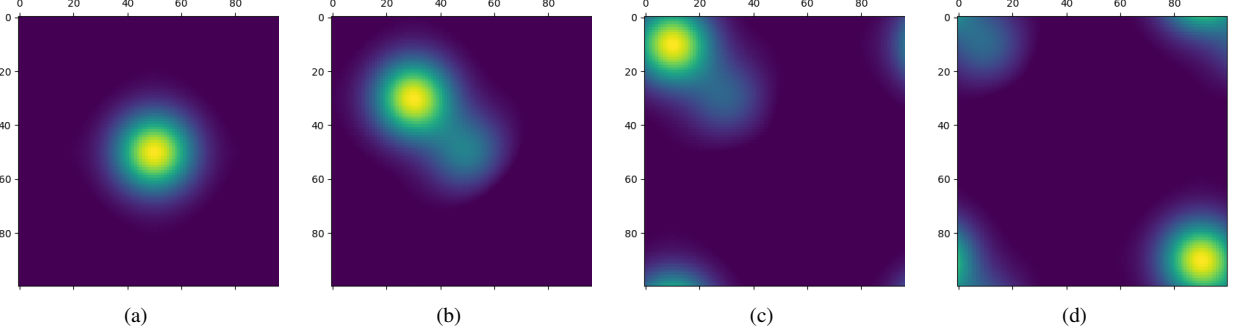


Figure 4: Activity and stabilization. The yellow color and blue color represent the high and low excitatory region separately. (a) Firstly, the network is injected energy in (50, 50). Then the energy is spread by synaptic weight profile and the activity bump is formed in the sheet. (b). After that, the network is injected in new position (30, 30). Then the internal dynamic is performed to stabilize whole network. The new excitatory region appear a highest bump and previous excitatory region remain a lower bump. (c) Similar to (b), the network is injected energy in (10, 10). (d)Similar to (b), the network is injected energy in (90, 90). Because of the periodic boundary, the excitatory bump appear in four corner of the network.

calculated as follows:

$$\begin{aligned}\Delta x_i^w &= \int_{t_i}^{t_{i+1}} |\nu(t)| \cdot \cos\alpha(t) dt \\ \Delta y_i^w &= \int_{t_i}^{t_{i+1}} |\nu(t)| \cdot \sin\alpha(t) dt\end{aligned}\quad (21)$$

where Δx_i^w and Δy_i^w are the translation of two directions in the world frame, $\nu(t)$ and $\alpha(t)$ are the translation velocity and head direction separately.

Then the translation in the world frame can be transformed into PhaseCAN by:

$$[\Delta x_i^g, \Delta y_i^g]^T = \mathbf{R}_{pg} \cdot \mathbf{R}_{wp} [\Delta x_i^w, \Delta y_i^w]^T \quad (22)$$

where Δx_i^g and Δy_i^g are the offsets in the PhaseCAN.

For a neuron ϵ_{xy} in (x, y) of the PhaseCAN, its firing rate ς_{xy} can be update by the path integration as follows:

$$\varsigma'_{xy} = \sum_{a=\delta x_o}^{\delta x_o+1} \sum_{b=\delta y_o}^{\delta y_o+1} \eta_{ab} \varsigma_{(x+a)(y+b)} \quad (23)$$

where η_{ab} is a 2×2 convolution kernel to compute the firing rate of ς_{xy} . Every item of η_{ab} can be acquired as follows:

$$\eta_{ab} = \frac{\sqrt{(a - \Delta x_i^g)^2 + (b - \Delta y_i^g)^2}}{\sum_{a=\delta x_o}^{\delta x_o+1} \sum_{b=\delta y_o}^{\delta y_o+1} \sqrt{(a - \Delta x_i^g)^2 + (b - \Delta y_i^g)^2}} \quad (24)$$

where $\delta x_o, \delta y_o$ are the rounded down integer offsets in the x and y directions of the PhaseCAN, they can be calculate as follows:

$$\begin{bmatrix} \delta x_o \\ \delta y_o \end{bmatrix} = \left[\lfloor \Delta x_i^g \rfloor \right] \quad (25)$$

where $\lfloor \cdot \rfloor$ represents the rounded operation.

A virtual path is generated in a 5×5 square virtual environment to simulate the animal's path. During this process, the velocity and angle of the virtual point was recorded and used to drive the proposed network. The properties of grid cell module are similar to Table.1. In addition, the world frame and the

frame of place cell firing space are set up identically. In other words, the rotation matrix \mathbf{R}_{wp} is the identity matrix and the translation vector ϖ is the zero vector.

In per time step, the offsets are calculated by Eq. (21). Then the firing rate of every neuron in the PhaseCAN can be updated by Eq. (22)-(25). The several snapshots of the network status during this process are depicted in Fig. 5. The excitatory bump continuously move in the network sheet. This demonstrates PhaseCAN can maintain the stability and perform the path integration. When the bump reach to the edges of the network sheet depicted in the Fig. 5(e) and Fig. 5(f), the bump will appear in opposite edge because of the periodic boundary condition.

To show the activity of single grid cell in the module, three neurons in the network are chosen to record their activity during the path integration. In addition, the parameters of network set up are similar to the Table.1. But the spacing of grid cell module is set to 1.20 in here. When the bump move through these neurons, the neurons acquire excitatory condition. By this way, the firing patterns of single grid cell are recorded depicted in the Fig. 6. The Figure shows that the firing patterns of single grid cell approximately are hexagonal. This is consistent with the properties of grid cells and experiment results(Hafting et al., 2005).

To further demonstrate the activities of single neuron in different grid cell module, we establish nine PhaseCAN with different spacing and orientation. Then the firing activities in same position of these networks are recorded with driving the networks using the moving path mentioned above. The results are shown in Fig. 7. Comparing the figures from left to right, the firing patterns are rotated with increasing orientation of the grid cell. In addition, the change of interval is consistent with the increasing spacing of the grid cell module. This demonstrates our proposed model can be applied in different properties of grid cells. In previous researches(Bush et al., 2015; ?), the gird-like patterns are used as accurate path integration. In here, the grid-like patterns are generated. But the patterns are obviously irregular and snatty. Although the patterns generated are consistent with the observation of the biological experiment(Hafting et al.,

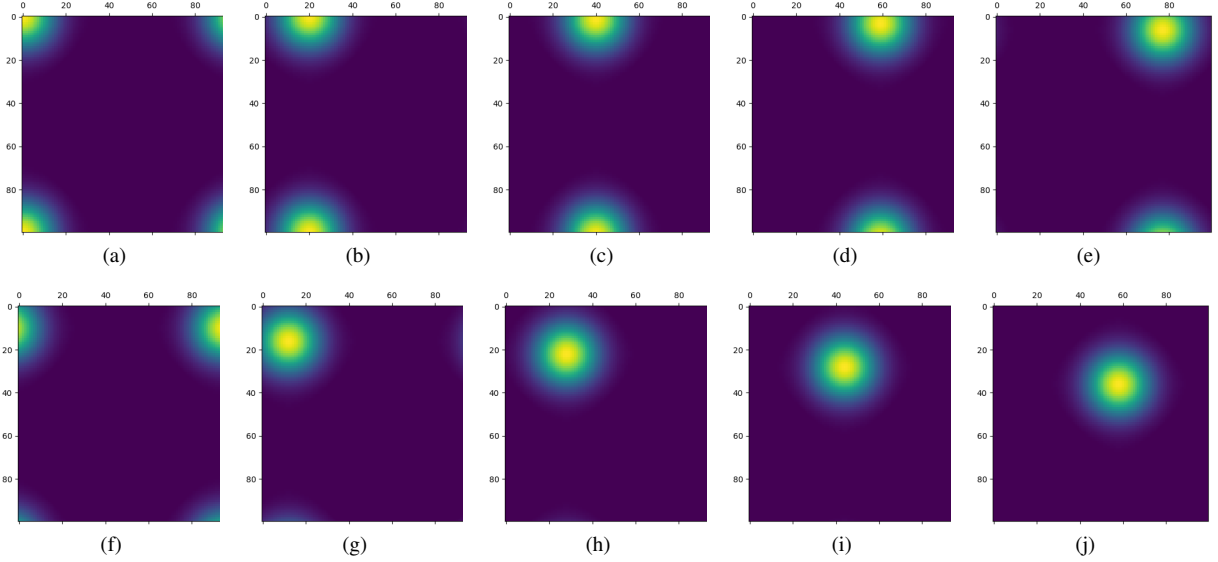


Figure 5: The snapshots of network status during the path integration. In the figure, different colors represent different firing rates of the neurons. The firing rates gradually decline through yellow to blue. In the beginning, as the (a) shown, the origin point is the $(0, 0)$ and so the corresponding neuron in the $(0, 0)$ is activated. Along the moving of virtual point in the environment, the excitatory bump begin to move. In addition, the snapshots are chosen per two time steps in here to better show the process.

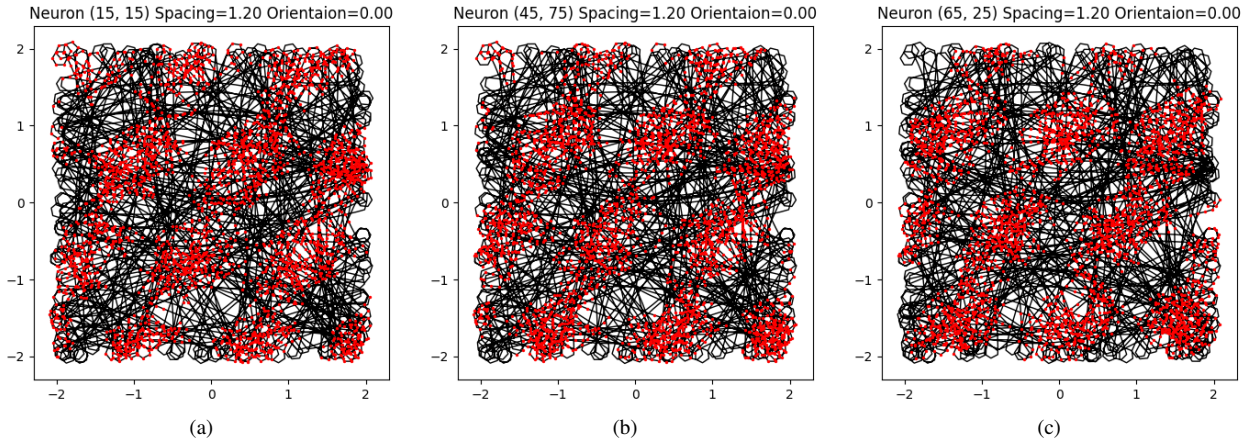


Figure 6: The firing patterns of the single grid cell in the different position of the PhaseCAN. The black lines in the three figures are the paths that are generated in the virtual environment. The red points represents the firing condition of single neuron. (a) The firing pattern of the neuron in the position $(15, 15)$ of the network. (b) The firing pattern of the neuron in the position $(45, 75)$ of the network. (c) The firing pattern of the neuron in the position $(65, 25)$ of the network.

2005), they are hard to use as a accurate path integration. According to our concept, path integration should be performed using a single grid cell module rather than a single grid cell.

To verify the ability of our model to perform path integration, several experiments are designed. We compare the performance of different PhaseCAN models that have different spacing of grid cell and different size of network in the Eq. (2). The results of experiment are shown in Fig. 8. In general, the error of path integration gradually increases with moving steps. For different spacing of grid cells, the error of bigger spacing is more obvious than the smaller in Fig. 8(a). In addition, the size of network also influence the deviation of path integration. The more neurons in the network can acquire the lower error of path integration in general. In here, the precise \mathcal{J} of path integration

can be described as follows:

$$\mathcal{J} \propto \frac{1}{s/N} = \frac{1}{\varrho} \quad (26)$$

where s represents the spacing of grid cells, N is the size of the network, ϱ is the ratio of s and N marked as network resolution ratio of CAN. According to the results of experiment depicted in Fig. 8, we infer that the precise of path integration is proportional to the network resolution ratio ϱ .

In general, the error of path integration is accumulated with iteration. To eliminate the error, the visual cues are introduced and correct the deviation. In our model, as Fig. 3 shown, the landmarks in the actual world are mapping to the network of place cells. Then the excitation in the place cell network is

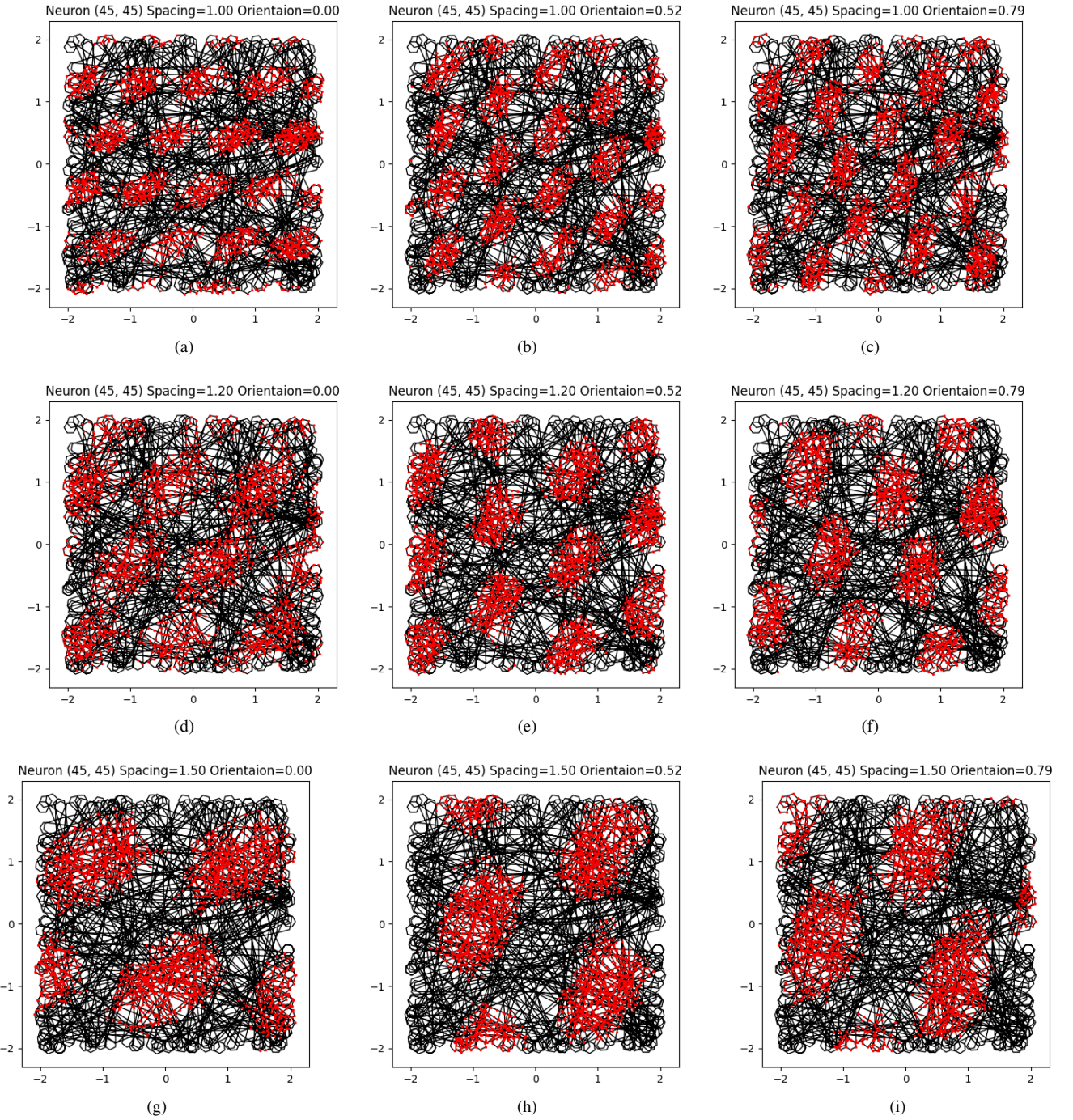


Figure 7: The firing patterns of the single grid cell in the different module but in same position of the PhaseCAN. The firing patterns in different orientation for the grid cell in same position of network are illustrated from left to right. With the increasing orientation of grid-cell module, the grid patterns incrementally rotate. The firing patterns with different spacing of the grid-cell modules are compared from top to bottom. The scales of single grid-cell firing patterns incrementally raised with the increasing spacing of grid-cell modules.

transformed and mapping to the firing space of grid cells. This can help the grid cell module to reduce the influence from accumulative error. In here, the excitation from place cell are injected into network of the grid cell module per 500 steps. The error of path integration is recorded per 100 steps to obviously show the difference between PhaseCAN model with and without

out feedback. This comparison is shown in Fig. 9. during the initial process, their errors all remains a low level. However, along the increasing steps, the PhaseCAN with feedback still can keep a low deviation. In contrast, the error of the PhaseCAN without feedback will increasingly increase. The results manifest our model have the ability to reduce the accumulated

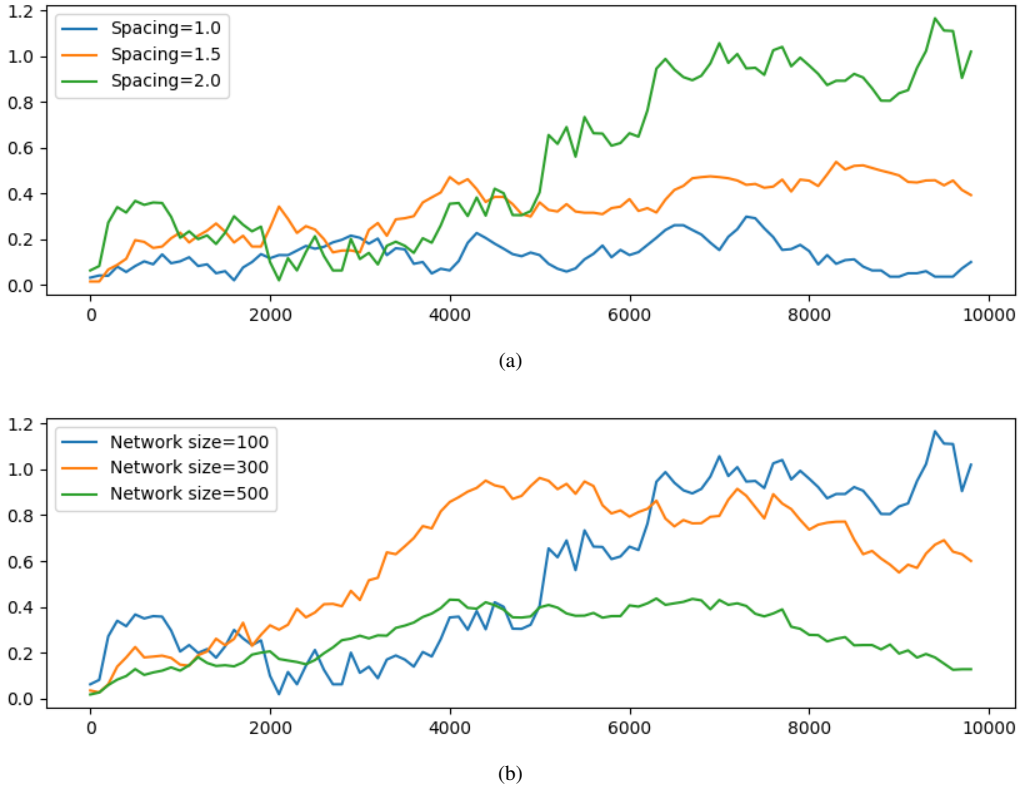


Figure 8: The error of path integration using PhaseCAN with iterations. The x-axis is the moving steps. (a) The error of path integration using different spacing in the PhaseCAN but same size of network, i.e., 100. (b) The error of path integration using different network sizes in the PhaseCAN but same spacing of grid cell, i.e., 2.0.

error with feedback.

To explore the ability of our model for path integration in long voyage, path integration is performed in longer steps. This is depicted in Fig. 10. In three different grid-cell modules, their error remains a scope even after 100000 steps without feedback from place cells. This also can partly explains why the rodent animals can return their dens even though they have go for a very long distance.

3. Discussion

The rodent animals have outstanding navigation ability(?). They can walk a long way and return their dens. This demonstrates they have the splendid ability of path integration. However, the latent mechanism of animals' navigation still be mysterious. The cognitive map is thought exists in the brain of animals(Tolman, 1948). It can provide a spatial representation for physical world to guide the animals. The discovery of place cells demonstrates the cognitive map may exist in the entorhinal-hippocampal circuitry(O'Keefe and Conway, 1978). After that, many spatial cells are found in this areas including head direction cells, speed cells, grid cells and so on. Specially, the grid cells have draw enormous attention because of their hexagonal firing patterns. The periodic firing patterns of grid cells in the MEC are thought to provide a compact code for location within large-scale space(Bush et al., 2015). In addition,

the general consensus is that grid cells provide a path integration input for place cells(McNaughton et al., 2006). So the grid cells are regarded as a key component for spatial representation in the entorhinal-hippocampal circuitry.

To explore the latent mechanism of grid cells, many computational models are designed. The main models of grid cells contain OI models(O'Keefe and Burgess, 2005; Burgess et al., 2007; Hasselmo et al., 2007; Pastoll et al., 2013; Burgess, 2008), CAN models(Fuhs and Touretzky, 2006; Burak and Fiete, 2009; Guanella et al., 2007; Shipston-Sharman et al., 2016; Couey et al., 2013) and single-cell adaptation models(Kropff and Treves, 2008; Si et al., 2012). They mainly focus on the firing activity of single grid cell and generate the hexagonal patterns from different perspectives using self-motion inputs or external cues. However, the evidence shows that the grid cells are ordered in discrete modules and each grid-cell module shares common spacing, orientation(Stensola et al., 2012; Rowland et al., 2016). In addition, recent research demonstrates the grid cells from a single module exist on a toroidal manifold like 2D CAN using enormous records from many hundreds of grid cells and topological data analysis(Gardner et al., 2022). Some new features are found from the views of grid-cell modules. The analysis shows that the positions in the toroidal manifold can map the positions of animals in the physical world and single grid cell prefers to be activated at a singular position on the torus(Gardner et al., 2022). Current CAN models(Fuhs

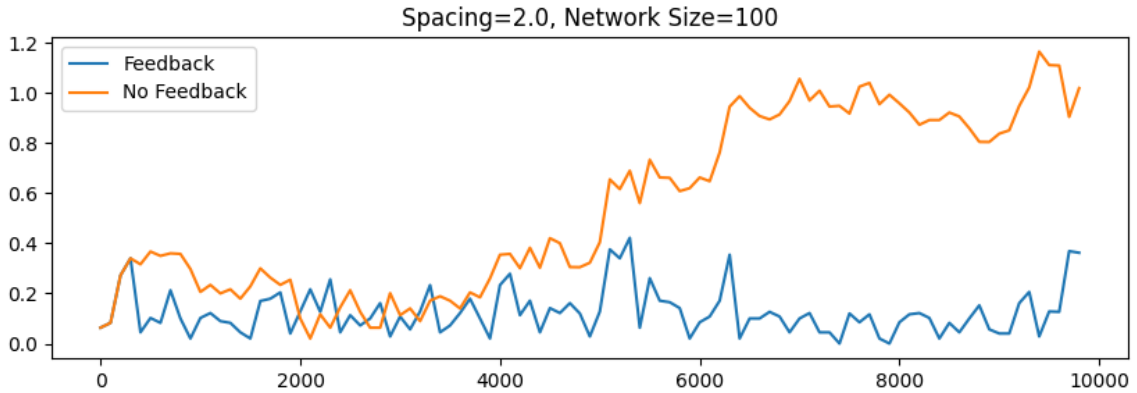


Figure 9: Error comparison of path integration with and without feedback.

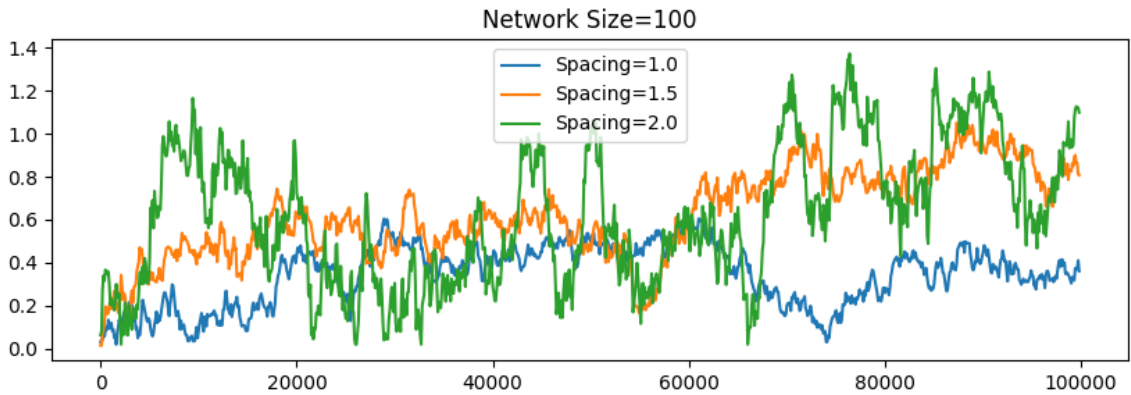


Figure 10: Error comparison of path integration without feedback in long voyage.

and Touretzky, 2006; Burak and Fiete, 2009; Guanella et al., 2007) can not be inconsistent with the analysis. Because the current CAN models are designed based on single grid cell and the properties of grid-cell modules do not be taken into account. Here, a CAN model for grid-cell module is proposed. It is driven by self-motion input of animals and receives the stimulation from external cues through place cells. Each neuron is preferentially active at a unique position on the torus and activated positions on the network represent the position of animals in the environment. This is consistent with the data analysis of Gardner et al. (2022). It demonstrates that our model supports the hypothesis about the grid-cell modules in the Gardner et al. (2022).

The key hypothesis for CAN model is that path integration can be performed by moving the bump in the network on the sheet(Fuhs and Touretzky, 2006). Many mechanisms are designed to shift the bump around a ring(Zhang, 1996) or over a sheet(Burak and Fiete, 2009). Comparing with other models, our model drives the attractor bump by transforming the self-motion inputs in the environment into grid-cell cognitive space. To simplify the process, the speed and head direction are calculated to acquire a minor translation. Then the translation is transformed into grid-cell cognitive space instead of transform-

ing directly speed and head direction. Another problem of path integration is the correction of accumulated errors by sensory cues. Our model resets the path integration using the inputs from place cells. The landmarks in the environment stimulate the place-cell network and then the activated bump in this network is transformed into grid-cell cognitive space. If the current bump on the grid-cell torus is different from the activated position from the external cues, the grid-cell CAN will be corrected and stabilized by intrinsic dynamic of network. The results of our model demonstrate the ability to achieve the path integration in Fig. 4 and Fig. 5. Then we explore the prominent ability for path integration and seek the factors that affect the precision of path integration. The results show that network resolution ratios and the feedback can affect the precision of path integration and correct the accumulated errors in Fig. 9 and Fig. 9. In addition, the results illustrate that our model can remain a low accumulated errors in long voyage only depending on own intrinsic network dynamic even when it lacks external cues. It also partly explains why the rodent animals have so prominent ability of navigation.

Current models of grid cells generate the hexagonal firing patterns and show the patterns on the 2D toroidal manifolds(Fuhs and Touretzky, 2006; Burak and Fiete, 2009;

(Guanella et al., 2007). Different from these models, our model more emphasizes the connection between grid-cell neurons on a singular module. So the firing patterns of grid cells can not be directly shown on the torus. To acquire the firing patterns of grid cells on the module, the firing activity of single neuron on the module need to be recorded with driving the whole model. The results are illustrated in Fig. 6. The activity of three neuron on the single module are recorded and show the hexagonal firing patterns. After that, activity of more neurons on different modules are recorded in Fig.7. They are consistent with the biological experimental results and show different spacing, orientation on different modules.

In summary, the PhaseCAN model was proposed for grid-cell module. Then the self-motion inputs are designed to drive the PhaseCAN model. In addition, to provides visual feedback for grid-cell module during the process of the path integration, the connection between place cell and grid cell is established. Simultaneously, the hexagonal firing patterns of single grid cell can be acquired by recording the firing activity of single neuron in the PhaseCAN model. Finally, we use our model to perform the path integration and comparing the results in different grid-cell properties and sizes of the PhaseCAN. The results point out that the network resolution ratio can influence the accuracy of the path integration. Furthermore, the results also manifests that our model can acquire outstanding performance even in the absence of external cues and on a large scale.

4. Declaration of Competing Interest

The authors declare that they have no known competing financial interests or personal relationships that could have appeared to influence the work reported in this paper.

5. Acknowledgments

References

- Alonso, A., Llinás, R.R., 1989. Subthreshold Na⁺-dependent theta-like rhythmicity in stellate cells of entorhinal cortex layer II. *Nature* 342, 175–177. doi:[10.1038/342175a0](https://doi.org/10.1038/342175a0).
- Amari, S.i., 1977. Dynamics of pattern formation in lateral-inhibition type neural fields. *Biological Cybernetics* 27, 77–87. doi:[10.1007/BF00337259](https://doi.org/10.1007/BF00337259).
- Brandon, M.P., Bogaard, A.R., Libby, C.P., Connerney, M.A., Gupta, K., Hasselmo, M.E., 2011. Reduction of Theta Rhythm Dissociates Grid Cell Spatial Periodicity from Directional Tuning. *Science* 332, 595–599. doi:[10.1126/science.1201652](https://doi.org/10.1126/science.1201652).
- Burak, Y., Fiete, I.R., 2009. Accurate Path Integration in Continuous Attractor Network Models of Grid Cells. *PLOS Computational Biology* 5, e1000291. doi:[10.1371/journal.pcbi.1000291](https://doi.org/10.1371/journal.pcbi.1000291).
- Burgess, N., 2008. Grid cells and theta as oscillatory interference: Theory and predictions. *Hippocampus* 18, 1157–1174. doi:[10.1002/hipo.20518](https://doi.org/10.1002/hipo.20518).
- Burgess, N., Barry, C., O’Keefe, J., 2007. An oscillatory interference model of grid cell firing. *Hippocampus* 17, 801–812. doi:[10.1002/hipo.20327](https://doi.org/10.1002/hipo.20327).
- Bush, D., Barry, C., Manson, D., Burgess, N., 2015. Using Grid Cells for Navigation. *Neuron* 87, 507–520. doi:[10.1016/j.neuron.2015.07.006](https://doi.org/10.1016/j.neuron.2015.07.006).
- Couey, J.J., Witoelar, A., Zhang, S.J., Zheng, K., Ye, J., Dunn, B., Czajkowski, R., Moser, M.B., Moser, E.I., Roudi, Y., Witter, M.P., 2013. Recurrent inhibitory circuitry as a mechanism for grid formation. *Nature Neuroscience* 16, 318–324. doi:[10.1038/nn.3310](https://doi.org/10.1038/nn.3310).
- D’Albis, T., 2018. Models of Spatial Representation in the Medial Entorhinal Cortex. Ph.D. thesis. doi:[10.18452/19306](https://doi.org/10.18452/19306).
- Doeller, C.F., Barry, C., Burgess, N., 2010. Evidence for grid cells in a human memory network. *Nature* 463, 657–661. doi:[10.1038/nature08704](https://doi.org/10.1038/nature08704).
- Domnisoru, C., Kinkhabwala, A.A., Tank, D.W., 2013. Membrane potential dynamics of grid cells. *Nature* 495, 199–204. doi:[10.1038/nature11973](https://doi.org/10.1038/nature11973).
- Fuhs, M.C., Touretzky, D.S., 2006. A Spin Glass Model of Path Integration in Rat Medial Entorhinal Cortex. *Journal of Neuroscience* 26, 4266–4276. doi:[10.1523/JNEUROSCI.4353-05.2006](https://doi.org/10.1523/JNEUROSCI.4353-05.2006).
- Fyhn, M., Hafting, T., Witter, M.P., Moser, E.I., Moser, M.B., 2008. Grid cells in mice. *Hippocampus* 18, 1230–1238. doi:[10.1002/hipo.20472](https://doi.org/10.1002/hipo.20472).
- Gardner, R.J., Hermansen, E., Pachitariu, M., Burak, Y., Baas, N.A., Dunn, B.A., Moser, M.B., Moser, E.I., 2022. Toroidal topology of population activity in grid cells. *Nature* 602, 123–128. doi:[10.1038/s41586-021-04268-7](https://doi.org/10.1038/s41586-021-04268-7).
- Giocomo, L.M., Hussaini, S.A., Zheng, F., Kandel, E.R., Moser, M.B., Moser, E.I., 2011. Grid Cells Use HCN1 Channels for Spatial Scaling. *Cell* 147, 1159–1170. doi:[10.1016/j.cell.2011.08.051](https://doi.org/10.1016/j.cell.2011.08.051).
- Giocomo, L.M., Zilli, E.A., Fransén, E., Hasselmo, M.E., 2007. Temporal Frequency of Subthreshold Oscillations Scales with Entorhinal Grid Cell Field Spacing. *Science* 315, 1719–1722. doi:[10.1126/science.1139207](https://doi.org/10.1126/science.1139207).
- Guanella, A., Kiper, D., Verschure, P., 2007. A model of grid cells based on a twisted torus topology. *International Journal of Neural Systems* 17, 231–240. doi:[10.1142/S0129065707001093](https://doi.org/10.1142/S0129065707001093).
- Hafting, T., Fyhn, M., Molden, S., Moser, M.B., Moser, E.I., 2005. Microstructure of a spatial map in the entorhinal cortex. *Nature* 436, 801–806. doi:[10.1038/nature03721](https://doi.org/10.1038/nature03721).
- Hasselmo, M.E., Giocomo, L.M., Zilli, E.A., 2007. Grid cell firing may arise from interference of theta frequency membrane potential oscillations in single neurons. *Hippocampus* 17, 1252–1271. doi:[10.1002/hipo.20374](https://doi.org/10.1002/hipo.20374).
- Jacobs, J., Weidemann, C.T., Miller, J.F., Solway, A., Burke, J.F., Wei, X.X., Suthana, N., Sperling, M.R., Sharan, A.D., Fried, I., Kahana, M.J., 2013. Direct recordings of grid-like neuronal activity in human spatial navigation. *Nature Neuroscience* 16, 1188–1190. doi:[10.1038/nn.3466](https://doi.org/10.1038/nn.3466).
- Killian, N.J., Jutras, M.J., Buffalo, E.A., 2012. A map of visual space in the primate entorhinal cortex. *Nature* 491, 761–764. doi:[10.1038/nature11587](https://doi.org/10.1038/nature11587).
- Koenig, J., Linder, A.N., Leutgeb, J.K., Leutgeb, S., 2011. The Spatial Periodicity of Grid Cells Is Not Sustained During Reduced Theta Oscillations. *Science* 332, 592–595. doi:[10.1126/science.1201685](https://doi.org/10.1126/science.1201685).
- Kropff, E., Carmichael, J.E., Moser, M.B., Moser, E.I., 2015. Speed cells in the medial entorhinal cortex. *Nature* 523, 419–424. doi:[10.1038/nature14622](https://doi.org/10.1038/nature14622).
- Kropff, E., Treves, A., 2008. The emergence of grid cells: Intelligent design or just adaptation? *Hippocampus* 18, 1256–1269. doi:[10.1002/hipo.20520](https://doi.org/10.1002/hipo.20520).
- Kunz, L., Schröder, T.N., Lee, H., Montag, C., Lachmann, B., Sariyska, R., Reuter, M., Stirnberg, R., Stöcker, T., Messing-Floeter, P.C., 2015. Reduced grid-cell-like representations in adults at genetic risk for Alzheimer’s disease. *Science* 350, 430–433. doi:[10.1126/science.aac8128](https://doi.org/10.1126/science.aac8128).
- McNaughton, B.L., Battaglia, F.P., Jensen, O., Moser, E.I., Moser, M.B., 2006. Path integration and the neural basis of the ‘cognitive map’. *Nature Reviews Neuroscience* 7, 663–678. doi:[10.1038/nrn1932](https://doi.org/10.1038/nrn1932).
- Moser, E.I., Moser, M.B., McNaughton, B.L., 2017. Spatial representation in the hippocampal formation: A history. *Nature Neuroscience* 20, 1448–1464. doi:[10.1038/nn.4653](https://doi.org/10.1038/nn.4653).
- O’Keefe, J., Burgess, N., 2005. Dual phase and rate coding in hippocampal place cells: Theoretical significance and relationship to entorhinal grid cells. *Hippocampus* 15, 853–866. doi:[10.1002/hipo.20115](https://doi.org/10.1002/hipo.20115).
- O’Keefe, J., Conway, D.H., 1978. Hippocampal place units in the freely moving rat: Why they fire where they fire. *Experimental Brain Research* 31, 573–590. doi:[10.1007/BF00239813](https://doi.org/10.1007/BF00239813).
- Pastoll, H., Solanka, L., van Rossum, M.C.W., Nolan, M.F., 2013. Feedback Inhibition Enables Theta-Nested Gamma Oscillations and Grid Firing Fields. *Neuron* 77, 141–154. doi:[10.1016/j.neuron.2012.11.032](https://doi.org/10.1016/j.neuron.2012.11.032).
- Rowland, D.C., Roudi, Y., Moser, M.B., Moser, E.I., 2016. Ten Years of Grid Cells. *Annual review of neuroscience* 39, 19–40. doi:[10.1146/annurev-neuro-070815-013824](https://doi.org/10.1146/annurev-neuro-070815-013824).
- Schmidt-Hieber, C., Häusser, M., 2013. Cellular mechanisms of spatial navigation in the medial entorhinal cortex. *Nature Neuroscience* 16, 325–331. doi:[10.1038/nn.3340](https://doi.org/10.1038/nn.3340).
- Shipston-Sharman, O., Solanka, L., Nolan, M.F., 2016. Continuous attractor network models of grid cell firing based on excitatory-inhibitory interactions. *The Journal of Physiology* 594, 6547–6557. doi:[10.1113/JP270630](https://doi.org/10.1113/JP270630).

- Si, B., Kropff, E., Treves, A., 2012. Grid alignment in entorhinal cortex. *Biological Cybernetics* 106, 483–506. doi:[10.1007/s00422-012-0513-7](https://doi.org/10.1007/s00422-012-0513-7).
- Stensola, H., Stensola, T., Solstad, T., Froland, K., Moser, M.B., Moser, E.I., 2012. The entorhinal grid map is discretized. *Nature* 492, 72–78. doi:[10.1038/nature11649](https://doi.org/10.1038/nature11649).
- Taylor, J.G., 1999. Neural ‘bubble’ dynamics in two dimensions: Foundations. *Biological Cybernetics* 80, 393–409. doi:[10.1007/s004220050534](https://doi.org/10.1007/s004220050534).
- Tolman, E.C., 1948. Cognitive maps in rats and men. *Psychological Review* 55, 189–208. doi:[10.1037/h0061626](https://doi.org/10.1037/h0061626).
- Welday, A.C., Shlifer, I.G., Bloom, M.L., Zhang, K., Blair, H.T., 2011. Cosine Directional Tuning of Theta Cell Burst Frequencies: Evidence for Spatial Coding by Oscillatory Interference. *Journal of Neuroscience* 31, 16157–16176. doi:[10.1523/JNEUROSCI.0712-11.2011](https://doi.org/10.1523/JNEUROSCI.0712-11.2011).
- Yartsev, M.M., Witter, M.P., Ulanovsky, N., 2011. Grid cells without theta oscillations in the entorhinal cortex of bats. *Nature* 479, 103–107. doi:[10.1038/nature10583](https://doi.org/10.1038/nature10583).
- Yoon, K., Buice, M.A., Barry, C., Hayman, R., Burgess, N., Fiete, I.R., 2013. Specific evidence of low-dimensional continuous attractor dynamics in grid cells. *Nature Neuroscience* 16, 1077–1084. doi:[10.1038/nn.3450](https://doi.org/10.1038/nn.3450).
- Zhang, K., 1996. Representation of spatial orientation by the intrinsic dynamics of the head-direction cell ensemble: A theory. *Journal of Neuroscience* 16, 2112–2126. doi:[10.1523/JNEUROSCI.16-06-02112.1996](https://doi.org/10.1523/JNEUROSCI.16-06-02112.1996).